Morphometry of Human Coronary Arterial Trees

S. AHARINEJAD,[1]* W. SCHREINER,[1] AND F. NEUMANN[2]
[1]Microcirculation Lab, Department of Anatomy, University of Vienna, A-1090 Vienna, Austria
[2]Department of Medical Computer Sciences, University of Vienna, A-1090 Vienna, Austria

ABSTRACT

Background: Some groups, including ours, have been generating arterial tree models using constrained constructive optimization (CCO). Arterial trees have been grown to arbitrary resolution without input of anatomical data. We performed this study to learn about the shortcomings that might have resulted from neglecting the anatomical data in CCO models.

Methods: In a total of 450 segments obtained from 4 human cast hearts, the ratio of bifurcating daughter segment radii ($0 < S_{bif} = r(2)/r(1) < 1$) was examined, which corresponds to the split of the total flow of the mother segment. For any complete bifurcation, where the radii of the parent segments and the radii of daughters were known, the area expansion ratio was computed ($A_{exp} = [r(1)^2 + r(2)^2]/ r(\text{parent})^2$).

Results: The bifurcating ratio was found to be distributed in a nonnormal fashion, with a median of 0.76. The average area expansion ratio A_{exp}, characterizing the change of cross-sectional area of the vasculature from proximal to distal, was 0.93 ± 0.26. The 'rate of branching' ($d(i)/(d(0))$ was defined by the segment diameter relative to the diameter of the root segment. Averaging the rate of branching over segments within each bifurcation level resulted in a decreasing function of bifurcation level.

Conclusions: This article provides new experimental data on branching geometry of coronary arteries (i.e., the trees evaluated in this study are purely delivering rather than conveying). Based on these facts, we suggest that the analytical bifurcation law in CCO might be replaced by the bifurcation rule obeyed on a stochastic basis only. Anat. Rec. 251:50–59, 1998.

Key words: heart; coronary arteries; area expansion ratio; corrosion casting; microscopy; scanning electron

Knowledge of coronary branching pattern is essential for the understanding of myocardial perfusion. There are many excellent studies done in different species which have dealt with measuring the coronary arteries' diameters, estimating their branching pattern, and based on these data, calculating the blood flow in the cardiac tissue (Zamir et al., 1984; Zamir and Silver, 1985; Zamir and Chee, 1987; Zamir, 1988; Zamir and Phipps, 1988; Bassingthwaighte et al., 1990; Gonzalez and Bassingthwaighte, 1990; Kassab et al., 1993). Corrosion casting has been applied most frequently to these questions. Intravital microscopy is the ultimate method that would allow us to directly observe the flow inside the cardiac tissue and would be therefore considered as a more appropriate model to gain insight into the flow properties of a definite tissue. This method, however, has its limits. The light delivery to the tissue and the imaging of the tissue are limited to 70 µm down the surface (Aharinejad et al., 1993a,b). In the case of the beating heart, the organ has to be isolated and perfused with an artificial pump. We were interested in learning about the architecture of small coronary arteries of the human heart rather than the analysis of the low-power images obtained under a dissecting microscope. This challenge resulted from our previous studies on computer simulations of arterial tree models by means of constrained constructive optimization (CCO;

*Correspondence to: S. Aharinejad, MD, Microcirculation Lab, First Department of Anatomy, University of Vienna, Währingerstr. 13, A-1090 Vienna, Austria. E-mail: seyedhossein.aharinejad@univie.ac.at

Received 4 March 1997; Accepted 29 December 1997

Schreiner, 1993; Schreiner and Buxbaum, 1993). This algorithm generates the structure of a vessel tree by the stepwise addition of new segments (represented by straight cylindrical tubes) and geometrical optimization of the tree. According to a given set of boundary conditions (perfusion area, perfusion pressure and flow) and constraints (bifurcation law) as well as a physiologically reasonable target (cost) function, arterial trees have been grown to arbitrary resolution (several thousand segments), without the input of any anatomical data (Fig. 1). Some morphometric properties of these model trees have been compared with experimental data, showing reasonably good agreement with regard to branching angles, pressure profiles, and segments' radii (Schreiner et al., 1994). However, considering the morphometry of model trees in detail, the occurrence of smallest vessels branching from large segments has been suspected to be an artifact (Fig. 1). In particular, there is no restriction in CCO models to the degree of asymmetry of bifurcations, as defined by the ratio of radii of branching segments. Statistically, the cumulative frequencies of a typical CCO tree showed 9% highly asymmetric bifurcations with a branching ratio of no more than 0.2 and 25% of bifurcations with a ratio of less than 0.4. A major concern of this study was therefore the analysis of the diameters of small coronary arteries in real arterial trees and their branching ratio at bifurcations. Furthermore, the area expansion ratio (VanBavel and Spaan, 1992) was calculated, and an analysis of the rate of branching (Zamir, 1988) was performed for the experimental data.

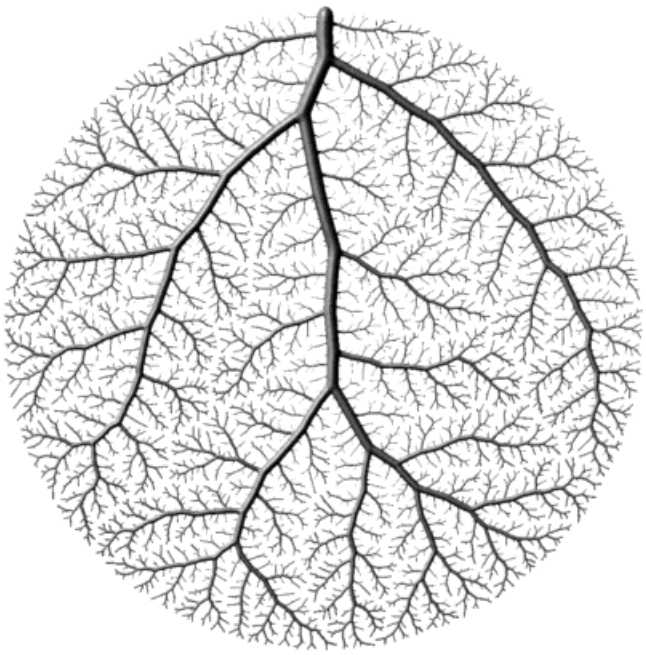

Fig. 1. Model tree generated by constrained constructive optimization, comprising 4,000 terminal and 3,999 bifurcating segments. The tree has been optimized for total intravascular volume, and the bifurcation law was given by $r(0)^3 = r(1)^3 + r(2)^3$, where $r(0)$, $r(1)$, and $r(2)$ are the radii of the bifurcating (mother) segment and of the daughter segments, respectively.

MATERIALS AND METHODS

Four human hearts obtained from cadavers were used for this study. The organs were obtained from three men and one woman aged 59, 61, 63, and 57 years. The cadavers were donated to the department of anatomy. Thanks to the cooperation of the department of pathology, we fulfilled the following criteria for obtaining hearts. (1) If death was caused by cardiovascular disease, as judged by the pathologist from the case history and after consulting the physician responsible for the patient's therapy shortly before death, the organ was excluded from the study. (2) We obtained organs within 4 hr after death. In Austria, biopsies of cadaver material can be obtained 3 hr after death. (3) Only those patients who were heparinized were included in the study. (4) Once the mentioned criteria were fulfilled, the heart was examined in situ. If coronary arteries had any macroscopic signs of atherosclerotic plaques, the organ was excluded from the study.

The heart was isolated and immediately processed. The initial segments of the coronary arteries were exposed. The ascending aorta was opened, and two glass cannulas with an outer diameter of 3 mm and an inner diameter of 2.5 mm were introduced into the right and left coronary arteries. The cannulas were ligated tightly just below the aortic root and connected to a two-way plastic connector (B. Braun Melsungen, Germany). One end of each tube was connected to a 50-ml syringe. The cannulated heart was then transferred into a large container containing 37°C warm tap water, with the heart being gently held under the water. We rinsed the cardiac vascular system by perfusing 50 ml heparinized (5,000 IU/L) Ringer solution (Leopold Pharma, Graz, Austria) at 37°C into each cannula using controlled manual pressure at 80 to 100 mm Hg. The efflux normally cleared when 80 ml lavage medium was perfused. Then, 80 ml Mercox (Ladd Industries, Burlington, VT) mixed with 8 g catalyst (55% benzoyl peroxide; Aharinejad et al., 1993a) was simultaneously perfused into the cannulas while the heart was gently held under water. With this technique, artifacts in the microvascular bed of the heart (which would occur due to the weight of heart) could be avoided. The perfused hearts were transferred into beakers containing tap water and put into an oven at 60°C, where they remained overnight to allow final polymerization of the resin (Aharinejad and Lametschwandtner, 1992). The water was then replaced gradually by a 5% KOH solution, and the organ was brought into an oven at 40°C. Soft tissue digestion was performed for 8 hr before the KOH solution was changed, and maceration was allowed to proceed for another 2 days. At that time, the maceration solution was gently washed out by using running tap water, and the casts were examined under the dissecting microscope. If any remnants of soft tissue were still present, the maceration was allowed to continue for 24 hr. Rinsing with tap water lasted 30 min, followed by rinsing with 5% formic acid for 30 min and several passages of rinsing with distilled water, each for 5 min.

Cast hearts were deeply frozen in distilled water at −30°C and first cut into two halves, parallel to the septum. Then, the left part of the heart was further cut at −20°C with a specially adapted circular saw into 3 × 2 cm blocks (Aharinejad and Lametschwandtner, 1992). The first cut was performed at the level of the first diagonal branch of LAD (left anterior descending artery), and the heart was then serially sectioned toward its apex. Cast blocks were freeze-dried (Lyovac, Germany) (freezing and freeze-drying the casts prevents spatial distortion that might occur during air drying) and mounted on copper foils and specimen studs using conductive bridges and silver paste

Fig. 2. SEM photo montage of a part of tree 4, belonging to a diagonal branch of the human left coronary artery. A major bifurcation of a mother artery is marked with an arrow. A blindly ending artery is marked with an arrowhead. x60.

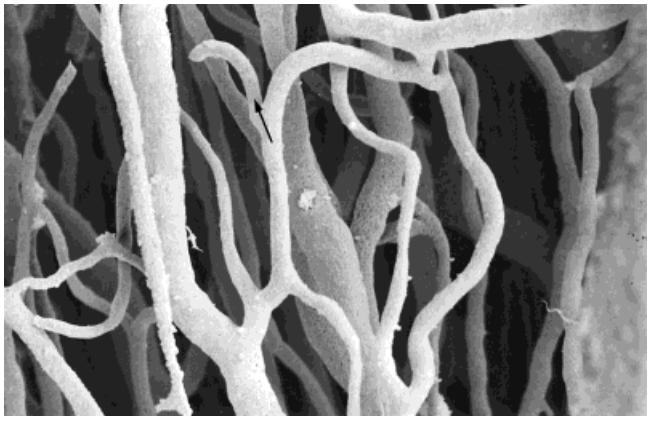

Fig. 3. SEM detail of a smaller branch of the artery shown in Figure 2. Note a blindly ending arteriole with blunted tip (arrow). The smaller arteries have a more tortuous course than the larger ones. x500.

(Lametschwandtner et al., 1980). The mounted cast was examined under the dissecting microscope. Using a micromanipulator (Leica, Vienna, Austria), those capillaries that obscured the view of myocardial arteries and their branches were removed. This procedure is possible because the arteries and their small branches have a blue color, whereas capillaries get a homogeneous white color when blue Mercox is used (as was the case in the present study). The casts were then sputter-coated with gold for 600 sec and analyzed in a Cambridge Instruments 90 scanning electron microscope (SEM, London, UK) at 15 kV accelerating voltage and 20 mm working distance (Aharinejad and Lametschwandtner, 1992; Aharinejad et al., 1993a,b).

In each cast heart, we followed the course of the left coronary artery under a dissecting microscope to find its most proximal diagonal branch. This diagonal artery and the segment it supplied were isolated under a microscope. The isolated cast was first examined under the dissecting microscope at higher magnification, and if larger branches were broken, the cast was excluded from the study. In this case, the most proximal marginal branch of the left circumflex coronary artery was dissected and prepared for SEM studies as described above. Microvascular 'tree'-

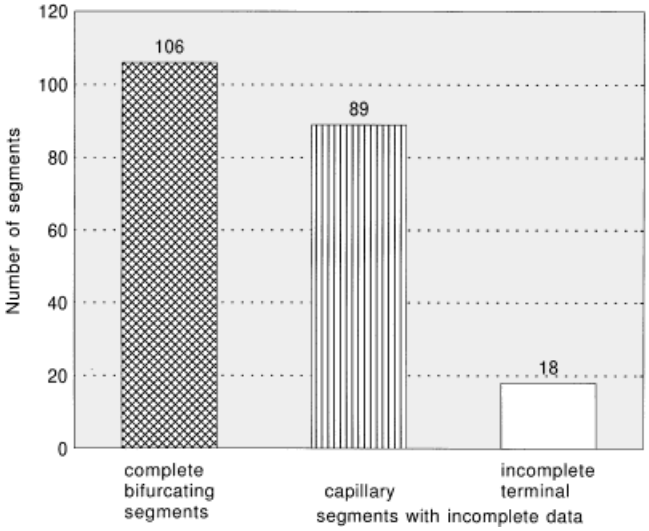

Fig. 4. Types of segments in a tree. A total of 213 segments comprising tree 4 were classified into bifurcating (cross-hatched), capillary (vertical lines), or incomplete terminal (white). Vertical axis: frequency.

TABLE 1. Global Morphometric Quantities*

	Tree 1	Tree 2	Tree 3	Tree 4
Number of segments	37	33	167	213
Number of segments with incomplete quantifications	18	15	86	107
Total length (mm)	0.72	0.63	1.76	4.08
Total surface (mm^2)	43.27	22.81	27.66	15.07
Total volume (mm^3)	1.54	0.75	0.98	0.82
Radius of root (mm)	0.071	0.066	0.071	0.109
Median branching ratio	0.678	0.722	0.818	0.737
Mean area expansion ratio	0.838	0.741	1.025	0.902
Rate of branching	0.720	0.651	0.789	0.801

*Total vascular length, total surface, total intravascular volume, mean branching ratio, and the mean area expansion ratio were computed from all segments of each tree for which the respective quantities were available. The sums given in the table thus represent lower bounds to the actual quantities of the complete trees. By comparing the number of segments with the number of incomplete quantifications, one can estimate the portion of cast fully accessible to quantification. The rate of branching was estimated according to Zamr (1988).

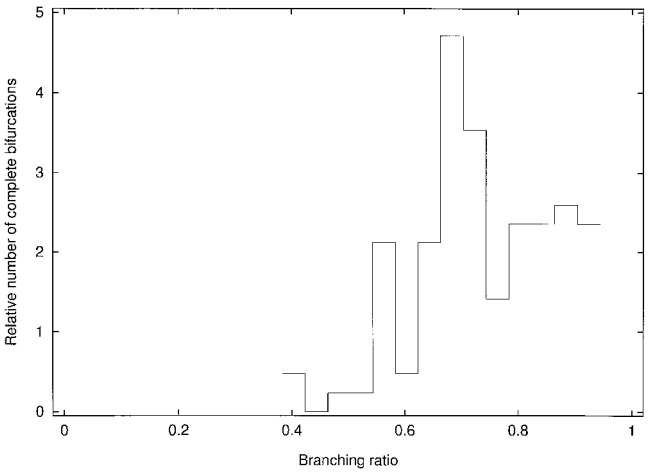

Fig. 5. Frequency distribution of branching ratio. Horizontal axis: branching ratio as calculated for tree 4 from equation 1 with equidistantly classified values of S_{bif}. Vertical axis: number of complete bifurcations within classes, divided by the total number of complete bifurcations of all four trees.

shaped corrosion casts were examined on the SEM screen using its measurement-calibration equipment. We focused on branches of coronary arteries. Vessels can be identified in cast preparations based on the shape and arrangement of endothelial cell nuclear imprints. Arteries have elongated nuclear imprints arranged parallel to the artery's long axis, whereas veins have roundish nuclear imprints with no recognizable geometry (Miodonski et al., 1976). The relief of endothelial cell nuclear imprints was also used to identify capillaries. The characteristic arrangement of imprints of endothelial cells' nuclei on arteries is no more visible on the surface of branching capillaries; in addition, capillaries rarely (if at all) reveal endothelial cell nuclear imprints (Aharinejad and Lametschwandtner, 1992). A vascular segment was defined as connecting any two consecutive branchings. For each vascular segment we evaluated two quantities: its diameter (the smallest) and length. In addition, each segment was morphologically classified as 'branching artery,' 'capillary,' or 'incomplete terminal vascular bed.' All branching mother segments definitely gave rise to two daughter segments, that is bifurcating, while triplications were never found. Capillary segments were identified according to their size, anastomosing and branching pattern, and histology (Rhodin, 1980; Aharinejad et al., 1990, 1992). Any vascular segment that could not be further traced in the cast (e.g., broken segments) was classified as incomplete. The one bifurcating segment representing the feeding vessel of each tree was called the 'root' segment and had no parent.

Morphometric Analysis

A total of 4 specimens (1 from each heart), which we will refer to here as trees 1 to 4, were examined. Trees 1 and 2 belonged to the marginal and trees 3 and 4 belonged to the diagonal branch of the left coronary artery. The trees consisted of 37, 33, 167, and 213 segments, respectively. In each tree a 'bifurcation level' was assigned to each segment by counting its number of proximal segments along the path toward the root of the respective tree, not including the segment itself. Bifurcation level zero was thus assigned to the root segment. We emphasize that each bifurcation increases the number of bifurcation levels regardless of the respective size of mother and daughter segments.

From diameters and lengths of individual segments, the total vascular length, the total surface, and the total intravascular volume of each tree were computed. For any complete vascular bifurcation, the branching ratio S_{bif} can be determined by dividing the radius of the smaller daughter, $r(2)$, by the radius of the larger daughter, $r(1)$, yielding a numerical value between 0 and 1.

$$S_{bif} = r(2)/r(1) \quad (1)$$

If the radii of both daughters and the radius of the parent segment are known, the area expansion ratio (VanBavel and Spaan, 1992) can be computed for any complete bifurcation as follows:

$$A_{exp} = [r(1)^2 + r(2)^2]/r(\text{parent})^2 \quad (2)$$

In the formula, r(parent), $r(1)$, and $r(2)$ denote the radii of the parent (mother) segment as well as that of the larger and smaller daughter segments, respectively. Averaging the area expansion ratios over a whole tree yields a measure characterizing the 'widening' of the vasculature from proximal to distal, and the change in (average) flow velocity is inversely proportional to A_{exp}. Of course, $A_{exp} = 1$ corresponds to constant flow velocity in parent and daughter segments.

RESULTS

Morphological Aspects

The casts analyzed were mostly of good quality and allowed us to follow the path of coronary microvessels (Fig. 2). When a mother vessel was identified, we searched for all branches that were visible on the SEM screen and started making a sketch. Next we followed the course of major branches at higher magnifications until we reached the capillary level. In doing this, a hallmark, (e.g., a major bifurcation of the mother vessel) (Fig. 2) was considered as a point to which the SEM scope was shifted when we wanted to follow other branches of the mother vessel running in the opposite direction of the first branch measured. Blindly ending vessels were observed both in the course of larger arterioles, ranging from 100 to 200 µm in diameter (Fig. 2), and in smaller arterioles, ranging from 15 to 50 µm (Fig. 3). These endings were mostly blunted, allowing the assumption that they were caused by contraction of contractile elements in the arterial wall rather than representing artifacts (i.e., broken vessels that would have a sharp edge). Bifurcations were present at all diameter levels, but true triplications were never observed (Figs. 2, 3). Smaller arterioles, ranging from 15 to 50 µm in diameter, had a more tortuous course compared with larger arterioles, which had a rather straight course (Figs. 2, 3).

Global Quantities

When calculating total vascular length as well as total surface and intravascular volume of each vessel tree, the results have to be understood with two restrictions. First,

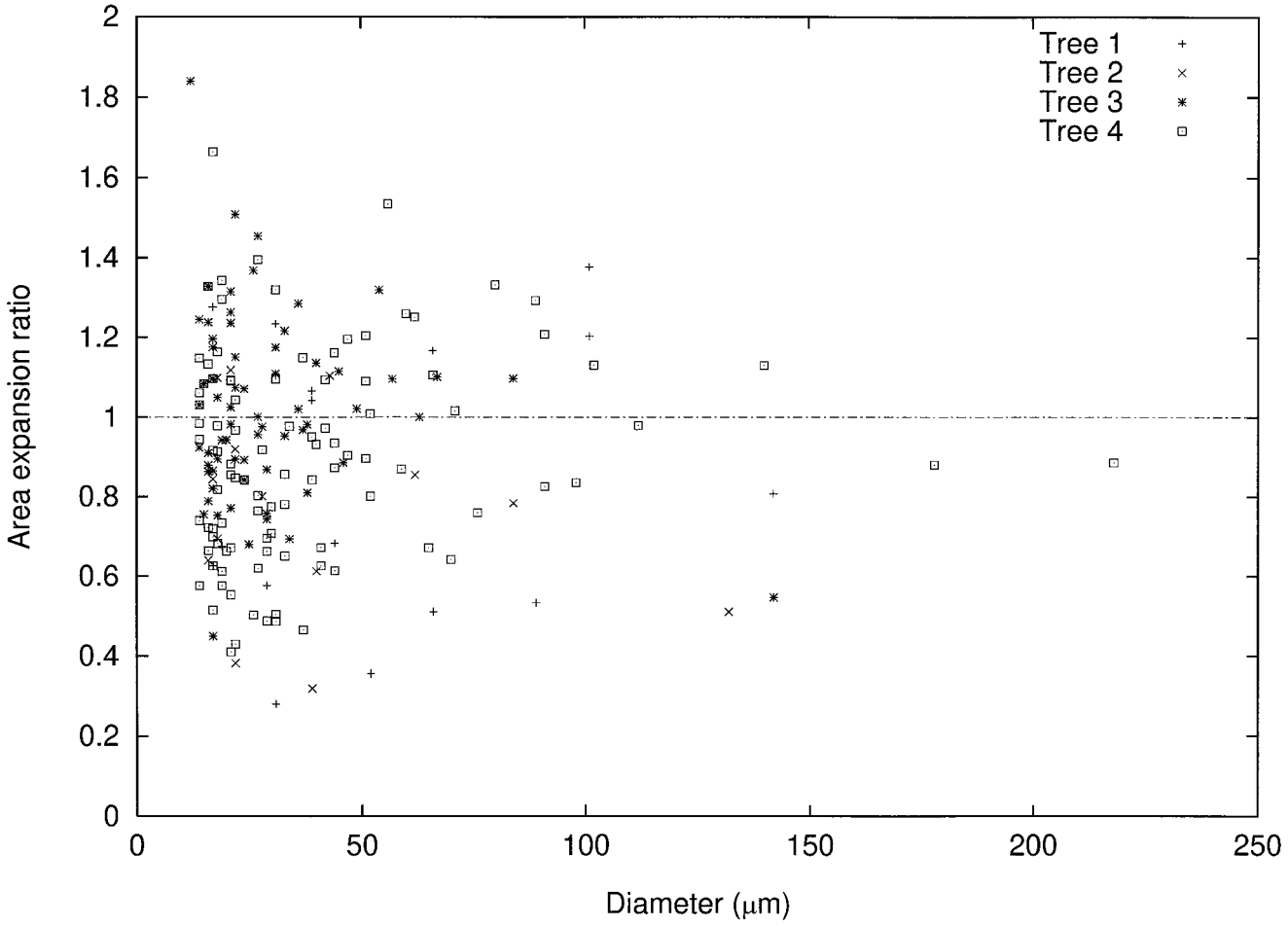

Fig. 6. Area expansion ratio versus parent diameter. Horizontal axis: parent segment diameter (μm). Vertical axis: area expansion ratio computed according to equation 2. A dashed line for $A_{exp} = 1$ corresponds to constant cross-sectional area across a bifurcation.

the vasculature distal to incomplete terminals is not included. Second, surface and volume cannot be estimated for a segment if either length or radius is missing. Therefore, capillaries had to be excluded from these calculations. To illustrate the frequency distribution of segments with regard to their type and suitability for quantification, see Figure 4. The first bar shows the number of bifurcating segments (i.e., branching arteries) for tree 4 (50%; the radius and length have been measured in each, 'complete quantification'). For capillaries (42%, represented by the second bar in Fig. 4), no lengths were obtained; hence, they belong to the group of 'segments with incomplete data.' The third bar indicates 8% of 'incomplete terminals,' which also contribute to the group of 'segments with incomplete data.' The proportions of segments with incomplete data were 49%, 45%, 51%, and 50% in trees 1, 2, 3, and 4, respectively (almost constant). The values of total vascular length, surface, and volume of all casts are shown in Table 1. Taking into account the number of (complete bifurcating) segments of trees and the radii of the respective root segments, total length, surface, and volume indicate some variability between the trees. For instance, comparing trees 1 and 3 shows that at equal root radius and a considerably smaller number of segments, the intravascular volume of tree 1 was 50% larger than that of tree 3.

Branching Ratio and Area Expansion Ratio

The geometrical measure of bifurcation symmetry S_{bif} (equation 1) will closely correspond to the split of the total flow of the mother segment into both daughter segments (VanBavel and Spaan, 1992). Repeatedly symmetrically bifurcating vascular structures with a high branching ratio (S_{bif} close to 1) can be classified as delivering vessel trees, whereas highly asymmetric structures with small branching ratios (S_{bif} close to 0) can be classified as conveying vessel trees (Zamir, 1988). Therefore, the frequency distribution of the branching ratio (see Fig. 5 for an example showing the branching ratio for tree 4) not only characterizes the degree of symmetry, but also the functional type of the tree structures examined in the present study. The overall frequency distribution with $0.2 < S_{bif} < 0.95$ was nonnormal (right skewed) with the median of 0.76 and showed a skewness of -1.09. Twenty-five percent of the S_{bif} values were higher than 0.85, indicating high symmetry. Another 25% were below 0.67, representing

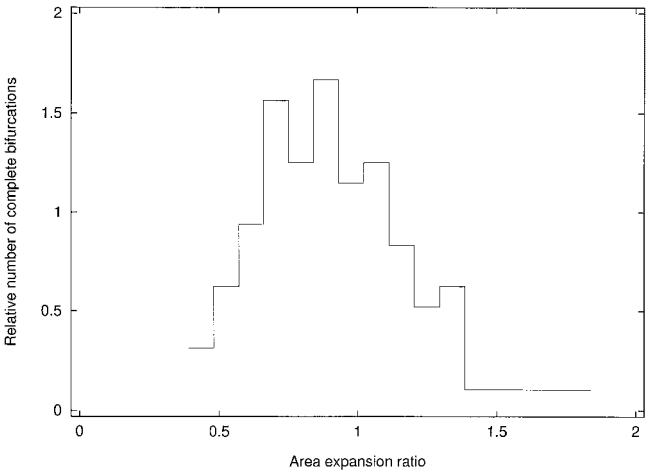

Fig. 7. Frequency distribution of area expansion ratio. Horizontal axis: area expansion ratio computed for tree 4 according to equation 2. Values for A_{exp} were equidistantly grouped into classes. Vertical axis: number of complete bifurcations within classes divided by the total number of complete bifurcations of all four trees.

bifurcations of only moderate or poor symmetry. Table 1 shows the median values for individual trees, ranging from 0.68 (tree 1) to 0.82 (tree 3).

For all complete bifurcations, the area expansion ratio A_{exp} (equation 2) was computed and plotted against parent segment diameter (Fig. 6). In addition, the frequency distribution of the area expansion ratio (Fig. 7) was computed over trees 1 to 4. The distribution is fairly normal (mean, 0.93; standard deviation, 0.26), centered around $A_{exp} = 1$ showing a right side tail up to approximately $A_{exp} = 2$ (skewness = 0.1). Individual mean values for all trees (ranging from 0.74 to 1.03) were calculated. These results are summarized in Table 1, which shows that for trees 1, 2, and 4 the average ratio A_{exp} was less than 1, indicating reduction of vascular diameter.

Path Analysis

Tracing a particular path within a tree from the root toward a specific terminal, the bifurcation level i increases by one from segment to segment. The diameter $d(i)$ of a segment can be expressed as a fraction of the radius of the root segment $d(i)/d(0)$. Because daughter segments [apart from a few exceptions where $d(i) = d(0)$] have smaller diameters than their respective parent segments, the ratio is a decreasing function of bifurcation level (Zamir, 1988). Figure 8 shows the ratios for all segments of trees 1 to 4 individually as dots. Averaging the ratio $d(i)/d(0)$ over all segments within each bifurcation level yields the curve shown in Figure 8. It might be stressed that each terminal segment of a tree defines a particular path, which usually has proximal parts in common with paths to other terminals.

If self-similarity prevails in a vascular tree, the relative shrinkage in radii should be constant across bifurcation levels, appearing as a straight line in semi-log plot of the same data (Fig. 9). The slope of the corresponding regression is a quantitative measure for the shrinkage, called 'rate of branching' (Zamir, 1988). Figure 9 shows the regression lines separately for each tree, and the quantitative results (last row in Table 1) show comparatively low values for the rate of branching. This result represents the blood-delivering (as opposed to blood-conveying; Zamir, 1988) function of all four trees. In other words, after branching and diminishing rapidly over a number of bifurcation levels, blood is directly supplied to the corresponding perfusion sites. This finding perfectly matches with the location of these trees within the microcirculation.

DISCUSSION

In the present study, four specimens of arterial trees with diameters of less than approximately 200 μm were morphometrically analyzed by using corrosion casts of human coronary arteries. Diameters and lengths of individual vessel segments were determined based on data obtained by SEM of casts. On the one hand, the present approach facilitated the classic description of global tree properties in terms of diameters, lengths, and their derived quantities. On the other hand, bifurcations and paths connecting the root with peripheral segments could be individually traced and statistically analyzed to globally characterize the structure of a whole tree. In detail, global quantities (such as sum of segmental lengths, total surface, and volume of each tree) were calculated from single segment measurements. The connective structure of the branching pattern was represented by the branching ratio, area expansion ratio, and path analysis.

With regard to the question of the degree of asymmetry (i.e., a lower bound of the diameter ratio characterizing any two branching segments at a bifurcation), the minimum branching ratio found experimentally was 0.21 and the 5% quantile was as large as 0.51. We therefore conclude that the rather frequent occurrence of heavily asymmetric bifurcations represents an artifact of model trees generated by constraint constructive optimization. Consequently, the CCO algorithm can be modified in such a way that a lower limit of the branching ratio is imposed as an additional constraint.

Considering the distribution of the area expansion ratio within an arterial, blood-supplying vessel tree, one would expect that on average, the total cross-sectional area would steadily increase and the vasculature would widen between subsequent bifurcation levels of the tree. The resulting decrease of flow velocity is assumed to allow for substrate and nutrition delivery to the surrounding tissue. In terms of the area expansion ratio, such a property of the tree would be represented by values of $A_{exp} > 1$ for the majority of bifurcations. Surprisingly, however, the area expansion ratio was less than 1 in almost 50% of the bifurcations (Figs. 6, 7). This result might not be necessarily interpreted as a constant narrowing of arterial trees toward the periphery. The following shall explain the alternatives that could shed light on this phenomenon. Analysis of variance performed between trees revealed that differences are statistically significant, with the significance mainly resulting from a relatively large number of observations rather than prominent differences between the trees. This is obvious from the extremely poor R^2 values of 0.16 for the branching ratio and 0.10 for the area expansion ratio.

Two conditions of regional vasoconstriction may bias the results obtained from our measurements. First, vasoconstriction and diameter reduction in the sense of precapillary sphincters of at least one daughter segment would

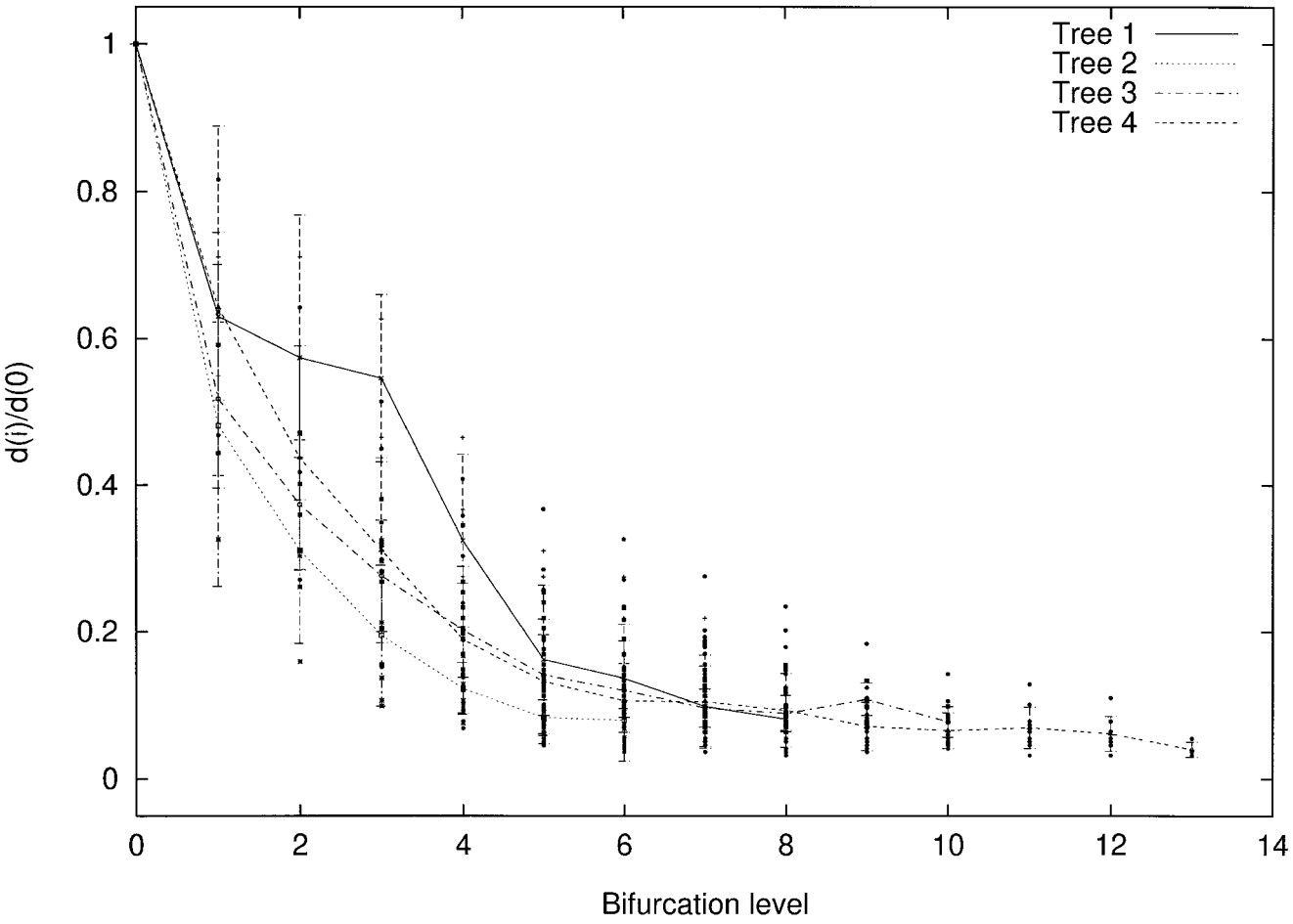

Fig. 8. Rate of branching versus bifurcation order. Horizontal axis: bifurcation order, where zero is assigned to the root element in each tree. Vertical axis: rate of branching in trees 1 to 4. Symbols denote the rate of branching for segments belonging to the same bifurcation order. Lines connect mean values of each tree, and bars denote standard deviations of individual values of each tree.

result in an underestimation of the 'active' daughter diameter compared with its 'passive' (i.e., nonactive) mother diameter. If this phenomenon occurs simultaneously in a large number of segments, the average area expansion ratio may be significantly reduced. Second, vasoactive agents (Bassingthwaighte et al., 1987; also see below) could transiently deprive relatively large areas of the microcirculation of blood flow. Hence, the vessels feeding these areas may have been completely closed and not filled with resin. Therefore, a certain number of anatomically existing bifurcations may have been omitted from the cast analysis. A segment originally representing the grandmother of a particular daughter segment may have erroneously been considered as its mother segment, which would bias the resulting area expansion ratio of the respective bifurcation toward a number that was too small.

A similar bias must be taken into account for the branching ratio representing the degree of symmetry of bifurcations. In this case, diameter reduction of only one daughter would bias the frequency distribution of S_{bif} toward smaller values, that is, toward asymmetry (Fig. 5). The biasing effect of a diameter reduction of both daughters, however, is unpredictable. In the path analysis, any underestimation of segment diameters may bias the shape of the curve (Fig. 8) toward low values of the diameter ratio $d(i)/d(0)$. If a certain number of vessels has actually been omitted from the analysis because they were totally closed at the time of perfusion, the frequency distribution of S_{bif} and the resulting curve of path analysis might be biased in a way that cannot be quantitatively estimated from the present data.

Another explanation for the smaller area expansion ratio of the daughter vessels versus their parent vessels might be that arteries can increase their diameters proximal to the apex of the bifurcation and decrease them distal to the bifurcation apex. Our measurements on branching arteries were done distal to the bifurcation apex; therefore, the potential widenings proximal to the bifurcation apex could have been disregarded. In this context, we may consider two facts. MacFarlanne and Roach (1977) described that the bifurcation geometry of arteries (isolated cerebral arteries in their study) can change depending on the pressure and subsequently alter the hemodynamic parameters. Yada et al. (1993) found, in their in vivo observations of the beating porcine heart, that while subendocardial arteries decreased their diameters during

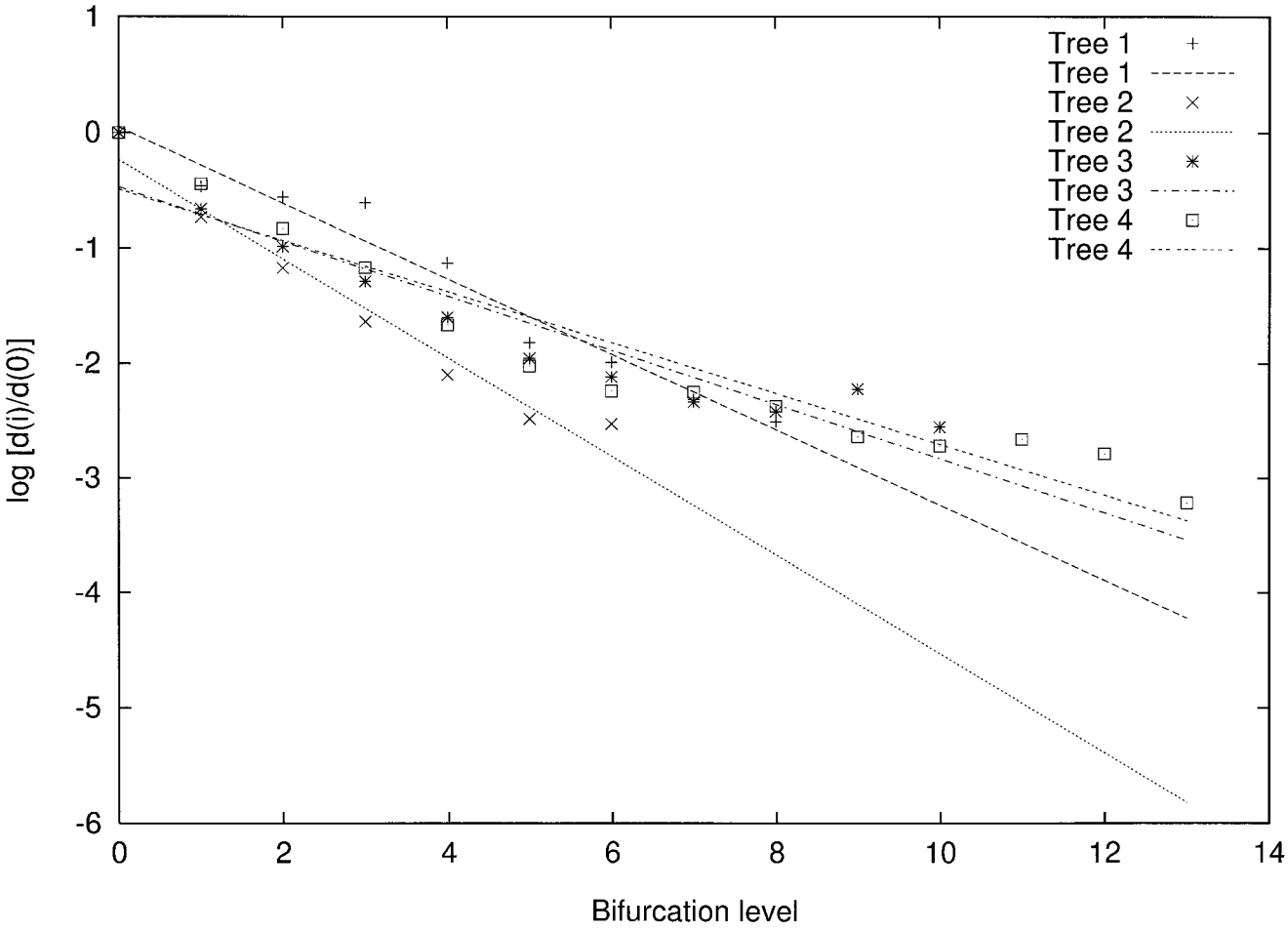

Fig. 9. Evaluation of rate of branching. For each subtree and bifurcation level, we averaged the ratios between segment radii and the radius of the root segment (mean values represented by tree symbols). After taking the log of the mean values, a linear fit was performed separately for each tree as indicated by the straight lines. The regression slope quantifies the amount of shrinkage in radius across bifurcations.

systole to about 20%, subepicardial arterioles changed their diameters very little. Our measurements started at the subepicardial arteries and then, as the artery supplied the deeper areas, continued toward the smaller subendocardial arteries. In other words, we are dealing with a pool of vessels that are cast in a moment at which (a) full perfusion of coronary arteries is guaranteed (i.e., perfusion pressure in physiological ranges), (b) the arteries are not compressed by the cardiac cycle (the heart had stopped beating in diastole), (c) the heart is denervated, and (d) a local accumulation of vasoactive substances (predominantly vasoconstrictors) can be expected. Changes of the arterial diameters caused by the factors mentioned above could bias the branching ratio representing the degree of symmetry of bifurcations. In addition, it is well documented in many studies that arteries change their tonus intermittently. When we cast a vascular tree, we obtain replicas that mimic a definite, short-time condition of the vascular tonus. These rapid changes of the vascular tonus and diameter would, in the case of short-term constrictions, lead to smaller diameters of the daughter vessels and result, at least in certain areas, in a lower cross-sectional area. In the following section, possible biological aspects of a potential vasoconstriction, which might have led at least in part to vasoconstriction, will be discussed.

The arteries supplying capillary networks have adjustable diameters. They display cyclic diameter variations, which in most cases are not attributed to periodic external influences such as cardiac or respiratory movements or propagation of pulse pressure. These periodic constrictions and dilations are called vasomotion. This term is preferentially used when the phenomenon is seen in vivo. Rhythmic contractions or tension oscillations have been used to describe similar phenomena observed in vitro (Gustafsson, 1993). The present study was done in vitro and hence the question arises as to whether the hypothesis on cyclic contraction of arteries might find validity. The simple answer is yes. Ross et al. (1980) have shown that isolated human coronary arteries show spontaneous phasic activity. This and many similar studies—for example, an (in vivo) model of denervated rabbit ear chamber (Wadström and Gerdin, 1993)—provide evidence that vasomotion is independent of innervation. Recent studies on this phenomenon show that endothelial-derived agents such as nitric oxide (NO) cause a subsequent generation of cGMP in the smooth muscle cells and hence activate oscillations in

membrane potential and tension, the oscillator itself being located inside the smooth muscle cell (Gustafsson, 1993; Gustafsson et al., 1993). Another study shows that vasomotion is not directly related to NO in conscious animals, whereas NO blockage stimulates vasomotion; however, simultaneous inhibition of cyclooxygenase and NO has no effect on arteriolar diameter during anesthesia (Bertuglia et al., 1994). We have recently shown that ET-1 focally constricts the veins and that it leads to widespread arterial contractions in the rat lung (Aharinejad et al., 1995). It is generally accepted that hypoxia and acidic environment can cause vasoconstriction which might be mediated by both ET (Aharinejad et al., 1995) and/or NO (Persson et al., 1990). We may conclude that (a) corrosion casting enables us to obtain reliable replicas of the microvasculature and to detect the effect(s) of vasoactive agents (Aharinejad et al., 1995, 1996), and (b) ET-1 might have been released from the endothelial cells of the coronary arteries and have caused contractions of their smooth muscle cells. Endothelin release could have been due to hypoxia caused by the postmortem cessation of blood flow and/or the subsequent lowering of the pH in vascular endothelial cells.

In almost 50% of the bifurcations, the daughter vessels revealed a joint cross-sectional area smaller than their parent vessels. VanBavel and Spaan (1992) found an area expansion ratio slightly larger than 1 (i.e. a mean value of 1.118 with a standard deviation of 0.302). In addition, a considerable number of bifurcations showed an area expansion ratio smaller than 1 in their model of porcine heart. The rate of branching, characterizing the shrinkage of segment radii as a function of bifurcation order, may be directly compared with the experimental work of Zamir (1988) on corrosion casts of the large coronary arteries in humans. In a linear plot, the shrinkage relative to the root segment appears as an exponentially declining curve. The value of the basis of that exponential function is a quantitative measure able to discriminate the functional characteristics of an arterial tree: conveying versus delivering. Within this concept, the trees evaluated in the present work were purely delivering, as appropriate within microvascular networks.

In CCO computer-generated model trees, a strict bifurcation law (Fig. 1) is obeyed analytically and hence the area expansion ratio is always larger than 1, if the exponent of the bifurcation law is chosen appropriately. Usually, a value of 3 is suggested in the literature (Sherman, 1981; Zamir, 1988). In contrast, the present results show that at least for the small arterioles of the terminal coronary bed, serious deviations from such a law seem to be inherent in real vessel trees. This finding is a new aspect regarding branching geometry and cross-sectional area and is in accordance with findings reported in a recent study by Zamir (1996), although his findings refer to the right coronary artery while ours focus on the left coronary artery. Zamir's study was published when this article was in revision. Hence, the parameters evaluated in this study will serve as a new basis for cardiovascular modeling. We may suggest to replace the analytical bifurcation law in CCO by the bifurcation rule obeyed on a stochastic basis only (e.g., with a predefined average area expansion ratio and a reasonable deviation allowed for individual bifurcations). Investigating the details of the concept of boundary conditions would require a separate methodological study of the CCO algorithm. This study is planned and will be performed in the near future.

LITERATURE CITED

Aharinejad S, Lametschwandtner A. Microvascular Corrosion Casting in Scanning Electron Microscopy. Techniques and Applications. New York: Springer, 1991: 12–31, 52–102.

Aharinejad S, Franz P, Böck P, Lametschwandtner A, Breiteneder H, Firbas W. Sphincterlike structures in corrosion casts. Scanning 1990;12:280–289.

Aharinejad S, Böck P, Lametschwandtner A, Firbas W. Scanning and transmission electron microscopy of venous sphincters in the rat lung. Anat. Rec. 1992;233:555–568.

Aharinejad S, MacDonald IC, MacKay CE, Mason-Savas A. New aspects of microvascular corrosion casting: A scanning, transmission electron, and high-resolution intravital video microscopic study. Microsc. Res. Tech. 1993a;26:473–488.

Aharinejad S, MacDonald IC, Schmidt EE, Böck P, Hagen D, Groom AC. Scanning and transmission electron microscopy and high resolution intravital videomicroscopy of capillaries in the mouse exocrine pancreas, with special emphasis on endothelial cells. Anat. Rec. 1993b;237:163–177.

Aharinejad S, Schraufnagel DE, Miksovsky A, Larson EK, Marks SC Jr. Endothelin-1 focally constricts pulmonary veins in rats. J. Thorac. Cardiovasc. Surg. 1995;110:148–156.

Aharinejad S, Schraufnagel DE, Böck P, MacKay CA, Larson EK, Miksovsky A, Marks SC Jr. Spontaneously hypertensive rats develop pulmonary hypertension associated with hypertrophied pulmonary venous sphincters. Am. J. Pathol. 1996;148:281–290.

Bassingthwaighte JB, Malone MA, Moffett TC, King RB, Little SE, Link JM, Krohn KA. Validity of microsphere depositions for regional myocardial flows. Am. J. Physiol. 1987;253:H184–H193.

Bassingthwaighte JB, Van Beek JH, King RB. Fractal branchings: The basis of myocardial flow heterogeneities? Ann. NY Acad. Sci. 1990;591:392–401.

Bertuglia S, Colantuoni A, Intaglietta M. Effects of L-NMMA and indomethacin on arteriolar vasomotion in skeletal muscle microcirculation of conscious and anesthetized hamsters. Microvasc. Res. 1994;48:68–84.

Gonzalez F, Bassingthwaighte JB. Heterogeneities in regional volumes of distribution on flows in rabbit heart. Am. J. Physiol. 1990;258:H1012–H1024.

Gustafsson H. Vasomotion and underlying mechanisms in small arteries. An *in vitro* study of rat blood vessels. Acta Physiol. Scand. 1993;149(Suppl. 614):1–44.

Gustafsson H, Mulvany J, Nilsson H. Rhythmic contractions of isolated small arteries from rat: Influence of the endothelium. Acta Physiol. Scand. 1993;148:153–163.

Kassab GS, Rider CA, Tang NJ, Fung YCB. Morphometry of pig coronary arterial trees. Am. J. Physiol. 1993;265:H350–H365.

Lametschwandtner A, Miodonski A, Simonsberger P. On the prevention of specimen charging in scanning electron microscopy of vascular corrosion casts by attaching conductive bridges. Mikroskopie 1980;36:270–273.

MacFarlanne TWR, Roach MR. Geometry of cerebral arterial bifurcations. Clin. Res. 1977;25:672A.

Miodonski A, Hodde K, Bakker KC. Rasterelektronenmikroskopie von Plastik-Korrosions-Präparaten. Morphologische Unterschiede zwischen Arterien und Venen. BEDO 1976;9:435–442.

Persson MG, Gustafsson LE, Wiklund NP, Moncada S, Hedquist P. Endogenous nitric oxide as a probable modulator of pulmonary circulation and hypoxic pressor responses *in vivo*. Acta Physiol. Scand. 1990;140:449–457.

Rhodin JAG. Architecture of the vessel wall. In: Bohr DF, Somlyo AP, Sparks HV Jr, eds. Handbook of Physiology. Section 2, Vol. 2. Bethesda, MD: American Physiological Society, 1980: 1–31.

Ross G, Stinson E, Schroeder J, Ginsburg R. Spontaneous phasic activity of isolated human coronary arteries. Circ. Res. 1980;14:613–618.

Schreiner W. Computer generation of complex arterial tree models. J. Biomed. Eng. 1993;15:148–150.

Schreiner W, Buxbaum PF. Computer optimization of vascular trees. IEEE Trans. Biomed. Eng. 1993;40:482–491.

Schreiner W, Neumann M, Neumann F, Roedler SM, End A, Buxbaum PF, Müller MR, Spieckermann P. The branching angles in computer-generated optimized models of arterial trees. J. Gen. Physiol. 1994;103:975–989.

Sherman TF. On connecting large vessels to small: The meaning of Murray's law. J. Gen. Physiol. 1981;78:431–453.

VanBavel E, Spaan JAE. Branching pattern in the porcine coronary arterial tree. Estimation of flow heterogeneity. Circ. Res. 1992;71: 1200–1212.

Wadström J, Gerdin B. Vasomotion in the totally denervated transplanted rabbit ear chamber. Microvasc. Res. 1993;46:103–105.

Yada T, Hiramatsu O, Kimura A, Goto M, Ogasawa Y, Tsujioka K, Yamamori S, Ohno K, Hosaka H, Kajiwa F. *In vivo* observations of subendocardial microvessels of the beating porcine heart using a needle probe videomicroscope with a CCD camera. Circ. Res. 1993;72:939–946.

Zamir M. Distributing and delivering vessels of the human heart. J. Gen. Physiol. 1988;91:725–735.

Zamir M. The structure and branching characteristics of the right coronary artery in a right-dominant human heart. Can. J. Cardiol. 1996;6:593–599.

Zamir M, Chee H. Segment analysis of human coronary arteries. Blood Vessels 1987;24:76–84.

Zamir M, Phipps S. Network analysis of an arterial tree. J. Biomech. 1988;21:25–34.

Zamir M, Silver MD. Morpho-functional anatomy of the human coronary arteries with reference to myocardial ischemia. Can. J. Cardiol. 1985;1:363–372.

Zamir M, Phipps S, Langille BL, Wonnacott TH. Branching characteristics of coronary arteries in rats. Can. J. Physiol. Pharmacol. 1984;62:1453–1459.